

The Malaria Parasite Progressively Dismantles the Host Erythrocyte Cytoskeleton for Efficient Egress^{*}

Melanie G. Millholland[‡], Rajesh Chandramohanadas^{‡¶}, Angel Pizarro[‡], Angela Wehr[‡], Hui Shi[§], Claire Darling[‡], Chwee Teck Lim[§], and Doron C. Greenbaum^{‡**}

Plasmodium falciparum is an obligate intracellular pathogen responsible for worldwide morbidity and mortality. This parasite establishes a parasitophorous vacuole within infected red blood cells wherein it differentiates into multiple daughter cells that must rupture their host cells to continue another infectious cycle. Using atomic force microscopy, we establish that progressive macrostructural changes occur to the host cell cytoskeleton during the last 15 h of the erythrocytic life cycle. We used a comparative proteomics approach to determine changes in the membrane proteome of infected red blood cells during the final steps of parasite development that lead to egress. Mass spectrometry-based analysis comparing the red blood cell membrane proteome in uninfected red blood cells to that of infected red blood cells and postrupture vesicles highlighted two temporally distinct events; (Hay, S. I., et al. (2009). A world malaria map: *Plasmodium falciparum* endemicity in 2007. *PLoS Med.* 6, e1000048) the striking loss of cytoskeletal adaptor proteins that are part of the junctional complex, including α/β -adducin and tropomyosin, correlating temporally with the emergence of large holes in the cytoskeleton seen by AFM as early ~35 h postinvasion, and (Maier, A. G., et al. (2008) Exported proteins required for virulence and rigidity of *Plasmodium falciparum*-infected human erythrocytes. *Cell* 134, 48–61) large-scale proteolysis of the cytoskeleton during rupture ~48 h postinvasion, mediated by host calpain-1. We thus propose a sequential mechanism whereby parasites first remove a selected set of cytoskeletal adaptor proteins to weaken the host membrane and then use host calpain-1 to dismantle the remaining cytoskeleton, leading to red blood cell membrane collapse and parasite release. *Molecular & Cellular Proteomics* 10: 10.1074/mcp.M111.010678, 1–12, 2011.

From the [‡]Department of Pharmacology, University of Pennsylvania, 433 S. University Ave, 304G Lynch Lab, Philadelphia, PA, 19104, USA; [§]Nano Biomechanics Laboratory, Division of Bioengineering and Department of Mechanical Engineering, National University of Singapore, Block E3, #05-16, 2 Engineering Drive 3, Singapore 117576

Received May 3, 2011, and in revised form, August 30, 2011

Published, MCP Papers in Press, September 8, 2011, DOI 10.1074/mcp.M111.010678

Malaria is a global disease causing at least 500 million new clinical cases per year, which result in more than 1 million deaths (1). Efforts to control malaria include small molecule-based prophylaxis and therapy, and insect vector elimination. However, the emergence of multidrug resistant *Plasmodium falciparum*, the cause of most malaria-associated deaths in humans, necessitates the discovery of novel antimalarials. *P. falciparum* traverses a complex life cycle involving sexual (mosquito) stages and multiple rounds of asexual division within the human host. The asexual blood stage begins when extracellular merozoites (initially released from the liver) invade red blood cells (RBCs)¹ in the blood stream. Over the next 48 h, intracellular parasites differentiate into the “ring” stage, metabolize hemoglobin (trophozoite stage), and replicate (schizont stage) to produce expanded populations of invasive merozoites that are released into the circulating blood after rupture of their host cell.

During this erythrocytic cycle, the malaria parasite causes major changes to its host cell. *P. falciparum* infection reduces deformability (2) and changes the adhesive properties of the host RBC, because of the appearance of knoblike protrusions on the surface (3–5) and specialized secretion of parasite proteins into the host cell (6, 7). Yet perhaps the most profound change to the RBC is its complete collapse at the end of the parasite erythrocytic cycle, as the newly replicated merozoites are released (8). For many years, parasite proteases have been thought to be important for rupture of malaria parasites from host cells (9): from initial inhibitor-based data, a two-step model of parasite rupture was proposed, requiring the activity of a cysteine and possibly a serine protease, as the general cysteine protease inhibitor E64 and the cysteine and serine protease inhibitors leupeptin and chymostatin inhibited PV and RBC plasma membrane rupture, respectively (10–12). More recently, several reports have implicated the involvement of three proteases in the rupture

¹ The abbreviations used are: RBC, red blood cell; iRBC, infected red blood cell; PV, parasitophorous vacuole; hpi, hours post-infection; AFM, atomic force microscopy; RPMI, Roswell Park Memorial Institute; PBS, phosphate-buffered saline; SERA, serine repeat antigen.

process: the parasite-derived proteases PfDPAP3 (13) and PfSub1 (14), and the human protease calpain-1 (15). In addition to proteolytic enzymes, it has also been established that osmotic forces (16), changes in parasite calcium flux (17), pore-forming proteins (18), and a kinase (19) are important for efficient egress of apicomplexan family parasites.

Although these studies have provided details on a variety of parasite proteins that act or are proteolytically processed during egress (20), we hypothesized that the parasite likely modifies host RBC proteins and specifically needs to destabilize the host cytoskeletal-membrane network to efficiently exit from the host cell. Thus, we were interested in a more comprehensive understanding of changes to the infected red blood cells (iRBC) membrane and cytoskeleton proteomes as the parasites prepare the host cell for rupture and merozoite exit.

EXPERIMENTAL PROCEDURES

Antibodies and Other Reagents—Monoclonal antibodies against calpain-1 and Band 3 were purchased from Sigma. Spectrin antibodies (α , β , and β C-terminal domain) were donated by Dr. David Speicher (Wistar Institute, Philadelphia, PA), Band 4.9 antibody was purchased from BD Biosciences and all the other antibodies (α -Adducin, Ankyrin-1, Flotillin-1, Stomatin, Actin, and CD47) were purchased from Santa Cruz Biotechnology (Santa Cruz, CA). Calpastatin was purchased from EMD Biosciences (San Diego, CA). Recombinant human calpain-1 was purchased from Calbiochem (San Diego, CA).

Cell Culture and Maintenance—*P. falciparum* (3D7) was grown under standard conditions in human RBCs supplemented with Albu-max in Roswell Park Memorial Institute (RPMI) medium (21).

Purification and Microscopic Analysis of the RBC-derived Vesicles Formed During Rupture—Schizont-stage parasites ~40 h post invasion (hpi) were purified from synchronous cultures using a SuperMacs magnet (Miltenyi Biotec Auburn, CA) and resuspended in culture medium. Once the majority of schizonts ruptured, as determined by Giemsa smears, the culture media was treated with protease inhibitor mixture and further collected by centrifugation at $1500 \times g$ for 10 min to remove residual uninfected and infected RBCs. This was followed by centrifugation at $5000 \times g$ for 30 min to remove extracellular merozoites. RBC membrane material, including small vesicles and loose membranes, resulting from rupture of parasites from RBCs was then purified from the residual media by ultracentrifugation (L8-70 M ultracentrifuge, Beckmann) at $200,000 \times g$ for 2 h at 4°C . The resulting RBC membrane material was then washed three times with phosphate-buffered saline (PBS). The post-rupture RBC vesicles isolated were stained with FM4-64 (Invitrogen, Carlsbad, CA) and DAPI for DNA. Samples were analyzed using a fluorescent microscope (Carl Zeiss Axioskop). Composite images were produced using Photoshop 6.0.1.

Atomic Force Microscopy—Thin smears were made on glass slides of uninfected RBCs, as well as from different stages of *P. falciparum* iRBCs such as of the ring, trophozoite, and schizont stages. These samples were first dried in a vacuum desiccator before conducting Atomic Force Microscopy (AFM). AFM imaging was performed on a NanoWizard II instrument (JPK Instruments AG Berlin, Germany). To image in the air or fluid contact mode, HYDRA6R-100N probes (AppNano Santa Clara, CA) were used. Height images were captured at a resolution of 512×512 pixels with a scan rate of 0.5–1 Hz (1 line/second). Images generated were then processed by NanoWizard image processing software (JPK instruments AG). To image the rupture-derived vesicles by AFM, a concentrated sample containing

enriched vesicles were allowed to bind to the surface of glass slides precoated with a commercially available lectin, Erythroagglutinin phytohemagglutinin (PHA-E, EY Laboratories San Mateo, CA) or a commercially available antibody that detects cytosolic domain of Band-3 protein for 1 h at room temperature as previously described (22). The slides were then washed twice with PBS and used before directly sending them for AFM imaging.

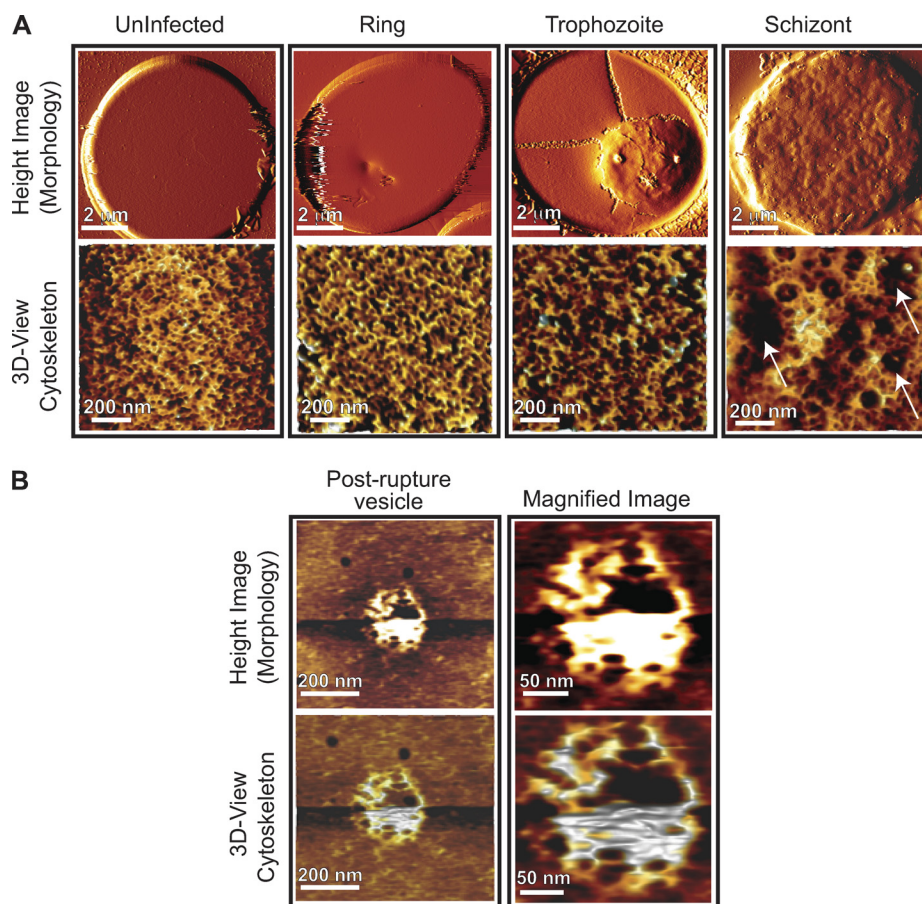
Preparation of RBC Membrane and Cytoskeletal Fraction—To prepare the iRBC membrane, schizont-stage iRBCs (~35–40 hpi) were purified using a magnetic column (Miltenyi Biotec). The parasites were then treated with 0.02% saponin in PBS for 10 min at 4°C and centrifuged at $1500 \times g$. The supernatant was centrifuged again at $4000 \times g$. This supernatant containing iRBC and parasitophorous vacuole (PV) contents was then ultracentrifuged ($200,000 \times g$ for 2 h at 4°C) to collect membranes. The membrane and cytoskeletal pellet was washed three times with PBS and subjected to a delipidation procedure by ethanol extraction (23) for 90 min prior to freezing with protease inhibitors (Roche) at -80°C . Finally, uninfected erythrocyte membranes were prepared as mentioned previously (23). RBCs were washed twice with PBS and subjected to hypotonic lysis in 5 mM lysis buffer (5 mM K_2HPO_4 , pH 8.0) containing protease inhibitors for 10 min in ice. Ghost membranes were collected by centrifugation of the lysate ($200,000 \times g$ for 2 h at 4°C). The pellet fraction containing the RBC membrane was washed until the pellet appeared as yellow or white ghosts. After delipidation, the membrane samples were frozen until used.

Protein Separation for MS—Aliquots from uninfected, iRBCs and postruptured vesicle membranes (~100 μg from each sample) were solubilized in Laemmli buffer under reducing conditions. After resolving on a 4–16% precast gradient gel (BioRad, Hercules, CA), polypeptides were stained with colloidal Coomassie. For mass spectrometric purposes, gel slices of 0.5 cm were excised from the entire length of the gel for each sample (total of 34 slices). Gel slices were destained with 20 mM ammonium bicarbonate and dried in 100% acetonitrile. Tryptic peptides from each gel slice were dried on a vacuum evaporator for mass spectrometry.

MS—Tryptic peptides were resuspended in acetonitrile and water. Peptides were separated by reverse phase using an Agilent 300 Extend-C18 column (3.5 mm, 2.1×150 mm). After a 6 min isocratic hold at 100% mobile phase A linear gradient was run over the next 33 min increasing the percent B (0.1% formic acid, 95% acetonitrile) to 60% all at a flow rate of 150 $\mu\text{l}/\text{min}$. Peptides were eluted online to a ThermoFinnigan LTQ mass spectrometer (ThermoFisher, San Jose, CA) and were ionized using electrospray ionization in the positive mode. Nitrogen was used as the sheath gas and collision induced dissociation experiments employed helium. Data dependent scanning was used to identify the top five most abundant ions over the range m/z 400–1500. Each of the five most abundant ions was then subjected to product ion scanning. (A mass tolerance of 2.0 Da for precursor ions and 1.0 Da for fragment ions was permitted). We used the extract_msn.exe tool from BioWorks version 2.x for generating peak lists from individual spectra.

Processing of MS Data—The raw tandem MS (MS/MS) data were searched through SEQUEST (TurboSEQUEST - PVM Slave v.27 (rev. 12), (c) 1998–2005) (Thermo Electron) against either a human RefSeq database (NCBI version updated 11/19/07) or the *Plasmodium* database (plasmodb.org). The databases were indexed using strict trypsin cleavage rules (K and R) with two maximum internal cleavage sites. Carbamidomethylation of cysteine residues (fixed modification) and oxidation of methionine (variable modification) were preset for the database searches. The SEQUEST output files were analyzed and validated by PeptideProphet (Version 3.0) as an automated method to assign peptides to MS/MS spectra. Postanalysis of the data was performed using the Trans Proteomic Pipeline with a peptide identi-

FIG. 1. AFM imaging demonstrates progressive cytoskeletal changes upon parasite development and merozoite egress. *A*, Uninfected RBCs and ring (10 hpi), trophozoite (25 hpi), or schizont (40 hpi)-infected RBCs were imaged using AFM. Processed images showed changes on the iRBC surface (mainly knob formation) by the trophozoite stage at 25 hpi (*upper Panel*). Extraction of cytoskeletal information (*lower Panel*) from AFM images showed increase in the mesh size of spectrin network by the trophozoite stage at 25 hpi, which expanded further by the schizont stage at 40 hpi. *B*, Post-rupture vesicles (48 hpi) were enriched by differential centrifugation and analyzed by AFM. Processed AFM images confirm a predominantly inverted, heterogeneous population of vesicles that contain adducts of the spectrin and actin-based cytoskeletal network.



fication probability cutoff of 0.05, which for all data sets corresponded to a false discovery rate <3%, and was <2% for most data sets. Data was further filtered and proteins with at least three peptides identified by SEQUEST were considered as positive “hits.” Multiple biological experiments were carried out to reproduce and confirm the proteomic results. GeneSpring Version 11.5 (Agilent) was used for generating heat map from the information obtained from MS analysis to analyze the relative distribution of proteins in gel slices among the three proteomes.

Western Blot Analyses—Protein samples were solubilized in Laemmli buffer, separated by SDS-PAGE and transferred to polyvinylidene difluoride membranes. Membranes were probed using available antibodies and visualized with corresponding secondary antibodies conjugated to horseradish peroxidase (Pierce). Hypotonic lysis and resealing of RBCs with calpastatin was done as previously published (15).

RBC Membrane Proteolysis by Calpain-1—Aliquots of 10 μ l (1 μ g/ μ l) erythrocyte membrane preparations were treated with 100 ng of purified calpain-1 in reaction buffer (20 mM HEPES, 10 mM dithiothreitol and 5 mM CaCl_2) for 30 min at 37 $^\circ\text{C}$. Negative controls were included by pre-incubating RBC membranes with calpastatin or EGTA prior to the addition of activated calpain. Samples were solubilized in Laemmli buffer under reducing conditions and resolved via SDS-PAGE and visualized by colloidal Coomassie. A fraction from each reaction was also resolved on SDS-PAGE, transferred to polyvinylidene difluoride membrane and probed for α - and β -Spectrins, Ankyrin-1, Stomatins, and Flotillin using commercially available antibodies.

Proteomic Protein Profiling—Protein degradation was assessed by creating “chromatograms” where the number of peptides identified

for each protein was plotted against the corresponding gel slice in which it was identified (as an approximation of molecular weight) from uninfected, infected, and postrupture RBC membrane proteomes. Majority of proteins peaked in gel slices that roughly corresponded to the nominal molecular weight among the three proteomes. Appearance of “peptide peaks” in lower molecular weight areas of the gel in the postrupture proteome and a corresponding absence or lessening of this peak in both uninfected and infected samples suggested protein degradation in the former sample. To further evaluate protein processing, peptides identified from proteolytic fragments were aligned manually against peptides identified from the full-length protein (identified at the correct molecular weight area of the gel), for several proteins that were found processed using chromatograms.

Adducin Immunofluorescence—Mixed-stage parasites were fixed in 4% paraformaldehyde/0.0075% glutaraldehyde for 1 h at room temperature, washed twice in dPBS, and permeabilized in 0.1% Triton X-100 for 10 min at 4 $^\circ\text{C}$. Parasites were washed twice in dPBS, blocked in 5% bovine serum albumin for 1 h with gentle mixing, then incubated with primary mouse anti-adducin- α antibody (Santa Cruz) at 1:250 dilution in 5% bovine serum albumin. Parasites were washed three times in dPBS, then incubated with Alexa 488-rabbit-anti-mouse antibody at 1:1000 dilution in 5% bovine serum albumin. Parasites were washed three times in dPBS, aliquoted onto slides and imaged on a Leica DM6000 Epifluorescence microscope.

RESULTS

Atomic Force Microscopy Reveals Progressive Macrostructural Modifications to the iRBC Cytoskeleton Upon Maturation and Exit of *P. falciparum* Parasites—We initially used AFM

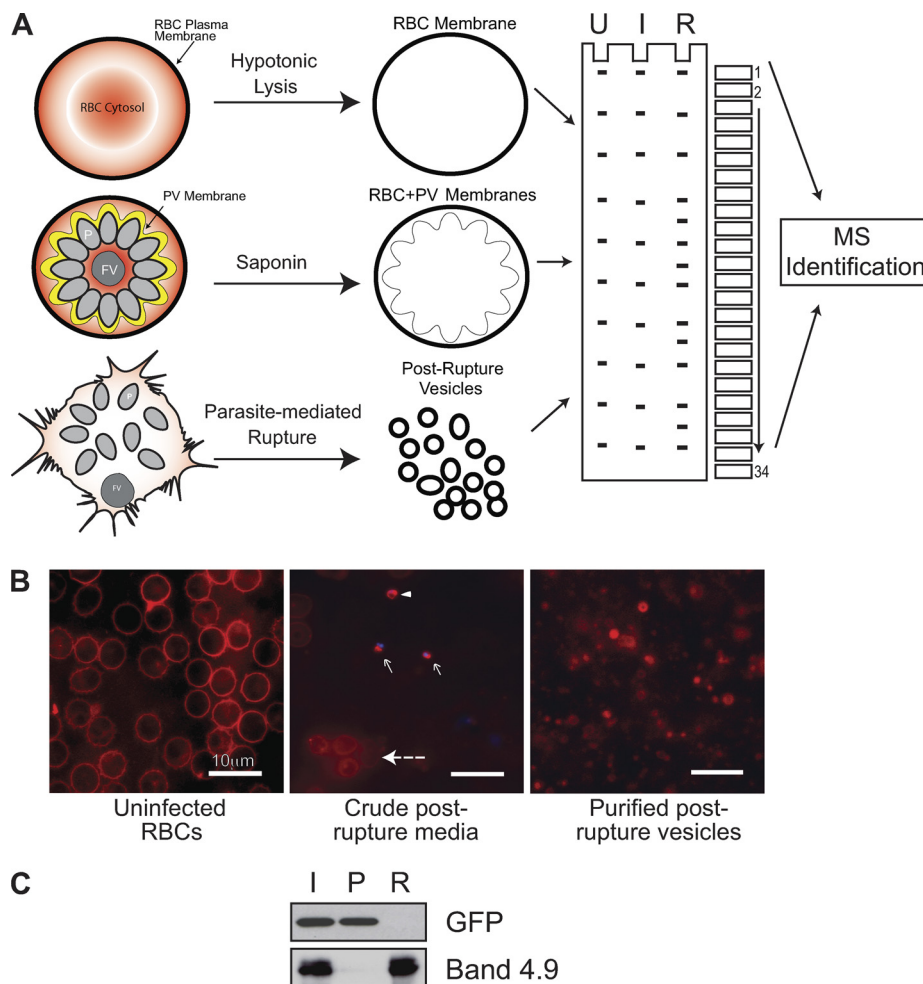


FIG. 2. Fractionation strategy for comparing uninfected RBC, iRBC, and postrupture vesicle membrane proteomes. To understand the global changes in the RBC membrane proteome upon parasite egress, parasite-infected (I) and postrupture vesicle membranes (R) were isolated and compared with uninfected RBC membranes (U). Newly replicated parasites (P) and the food vacuole after schizogony (FV) are also shown. **A**, Uninfected RBC membranes were prepared by hypotonic lysis and ultracentrifugation. The iRBC membrane proteome was prepared by saponin treatment of magnet-purified schizonts and ultracentrifugation. To prepare postrupture vesicle membranes, we used a differential centrifugation strategy to purify vesicles from media after parasite egress (see methods for more details). All the samples were solubilized in Laemmli buffer, resolved by SDS-PAGE and visualized by colloidal Coomassie staining. Thirty-four slices were excised from each proteome for analysis by mass spectrometry. **B**, To illustrate the efficiency of the fractionation strategy, the purification of postrupture vesicles was visualized by microscopy. Each fraction was stained with FM4-64 for membrane staining and DAPI for DNA. Panel 1: Uninfected RBCs; Panel 2: crude media just after parasite rupture from iRBCs containing merozoites (*arrow marks*), post-rupture vesicles (*arrowheads*) and intact RBCs (*broken line*); Panel 3: purified post-rupture vesicles derived from parasite egress. **C**, Selective enrichment of iRBC membranes from parasite material was also confirmed by Western blot analysis using a transgenic parasite line expressing cytosolic GFP. Protein from whole iRBCs (I), purified parasite cells fractionated by low speed centrifugation from saponin-treated iRBCs (P), or post-rupture vesicles fractionated from media after parasite egress (R) were separated by SDS-PAGE. Efficient isolation of iRBC membrane material was determined by western using a parasite cytoplasmic marker (anti-GFP) and a human RBC membrane marker (anti-Band 4.9).

imaging to look at structural changes to the iRBC surface and cytoskeleton during parasite development and egress. AFM images demonstrated major changes in morphology and appearance of the iRBC plasma membrane as shown by the knoblike protrusions, which are known to contribute to increased cytoadherence of parasitized cells (Fig. 1A, upper panel). However, during early schizogony (~35 hpi), large holes appeared in the cytoskeleton, with a corresponding increase in mesh size of the cytoskeletal network (Fig. 1A,

lower panel). This data suggests that structural changes and perhaps destabilization of the host cytoskeleton starts as early as ~35 hpi, much earlier than the actual time of parasite egress.

It has been established that at the time of parasite exit, the iRBC membrane collapses and forms postrupture vesicles ~one-tenth the size of an intact RBC (8). We enriched these postrupture vesicles by differential centrifugation and analyzed them by AFM (Fig. 1B). The vesicles, being highly fragile,

were allowed to bind to a glass slide precoated with PHA-E for stable AFM analyses. The postrupture vesicles were nonhomogeneous with sizes ranging from 200 to 800 nm in diameter. A majority of them appeared to be inverted as they bound efficiently to slides precoated with an erythrocyte band-3 antibody that has a luminal epitope (data not shown). AFM imaging showed clear evidence of disruption of the cytoskeleton mesh; however as these vesicles degraded rapidly, it was difficult to perform more specific imaging experiments.

Proteomic Analysis of Changes to the Host Membrane Proteome During Parasite Egress—We employed a proteomic approach to understand the molecular basis for the large changes in the iRBC cytoskeleton upon schizont maturation and egress, highlighted using AFM imaging. Three proteomes were compared via mass spectrometry-based analysis: (1) the plasma membrane proteome from uninfected RBCs, (2) the RBC/PV membrane proteome from iRBCs prior to parasite egress (~40 hpi), and (3) the RBC/PV membrane proteome isolated from iRBC postrupture vesicles. Although there certainly could be important cytosolic protein modifications during parasite egress, changes in the soluble proteome were largely obscured by hemoglobin, thus we specifically analyzed proteins in only the membrane fractions.

We developed a differential fractionation strategy to isolate these three host membrane proteomes (Fig. 2A). Uninfected RBC membranes were isolated by hypotonic lysis followed by ultracentrifugation. To isolate extraparasitic membranes (PV/RBC) from iRBCs, magnet-purified schizonts were separated from uninfected RBCs (24), then treated with saponin, which at low concentrations (0.02%) selectively permeabilizes the RBC/PV sparing the parasite plasma membrane (15). The RBC/PV membranes were then enriched by low speed centrifugation to remove whole parasite cells and further isolated by ultracentrifugation as described elsewhere (15). To isolate postrupture vesicle membranes from iRBCs, highly synchronous cultures of late-stage iRBCs were magnet-purified and allowed to naturally egress in culture media. Extracellular merozoites were then separated from culture media (containing postrupture membrane vesicles) by low speed centrifugation ($1500 \times g$). Post-rupture membrane vesicles were then isolated from the media by ultracentrifugation at $200,000 \times g$ for 2 h. For comparison, we show FM4-64 stained images of uninfected RBCs; parasite culture media collected immediately after rupture that contains both intact uninfected RBCs and postrupture vesicles (red), as well as released merozoites stained with Hoechst (blue); and purified postrupture vesicles purified from the media after parasite egress (red) (Fig. 2B). We observed little parasite contamination in either the iRBC membrane preparation or the samples enriched for postrupture vesicles. To confirm that we achieved purification of extraparasitic membrane material, we show the enrichment of the RBC membrane marker Band 4.9 and the concomitant loss of GFP from a parasite line expressing cytosolic GFP (Fig. 2C).

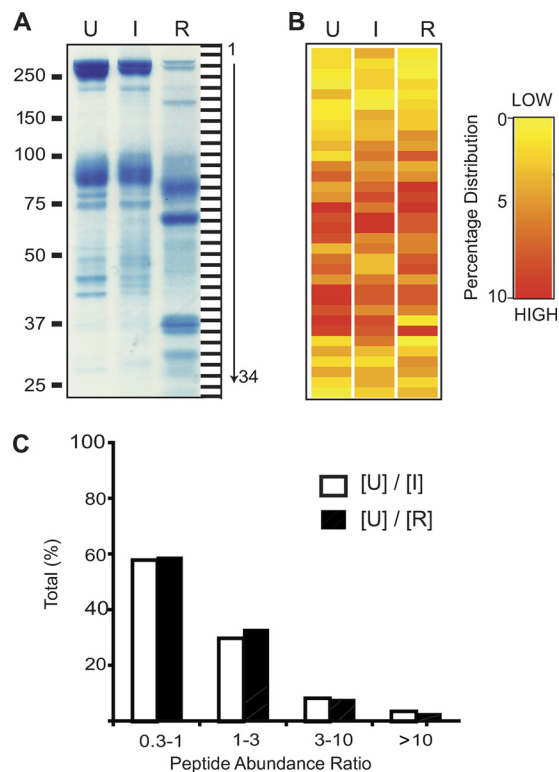


FIG. 3. Comparative proteomic analysis of the RBC membrane proteome during parasite egress. A, iRBC membranes (I) and postrupture vesicles derived from parasite egress (R) were isolated and compared with uninfected RBC membranes (U). Samples for the proteomic analysis were resolved on a 4–12% SDS-PAGE gel and stained with colloidal Coomassie. 34 slices were excised from each sample lane, digested with trypsin, extracted, and analyzed by LC/MS/MS mass spectrometry-based sequencing. The overall migration pattern for the post-rupture vesicle membrane proteome was different, as the characteristic high molecular weight spectrin doublet appeared to be degraded and with the appearance of more small molecular weight bands. B, Peptides from each gel slice were sequenced by mass spectrometry and the percentage distribution of identified proteins through the SDS-PAGE lanes for all samples (U, I, and R) were expressed in a heat map format. Red color indicates high percentage of peptides per protein (10%) whereas yellow indicates minimum (0%). This representation indicates that proteins were well-distributed throughout the SDS-PAGE gel. C, Spectral counting was used to compare the relative abundance of each protein from the three proteomes. The total number of peptides was summed for each identified protein in the iRBC and post-rupture vesicle proteome samples and was individually compared with the uninfected preparation to determine fold changes in relative protein abundance among the three proteomes. The abundance of most proteins remained similar (within a threefold difference) among the three proteomes, whereas a small proportion (~10%) showed markedly lower abundance in the postrupture vesicle proteome.

To identify and compare proteins from these three proteomes we employed an SDS-PAGE/MS approach akin to the gel liquid chromatography (LC)-MS/MS approach used by the Mann group (25), in which samples were first separated by one-dimensional SDS-PAGE, then individual gel slices across the entire lane were excised and subjected to LC/MS/MS

Host Cytoskeleton Changes during Malaria Parasite Egress

TABLE I

Proteins that are absent or reduced in iRBC and/or postrupture vesicle membranes. List of high abundance proteins that were identified in the uninfected RBC membranes and absent or reduced in the iRBC and postrupture vesicle membrane samples

Protein	Total Peptide Count			Function
	[U]	[I]	[R]	
Adducin 1 isoform d	246	-	-	Cytoskeletal associated
Adducin 2 isoform a	165	-	-	Cytoskeletal associated
CD47 antigen isoform 2	48	12	-	Surface Receptor
Rh blood group D antigen	37	3	-	Surface Receptor
Adducin 1 isoform a	32	-	-	Cytoskeletal associated
Galectin-3	29	-	-	Surface Receptor
RACH1	18	-	-	Transmembrane Transporter
Rab35	16	-	-	GTPase
Tropomyosin 1 alpha	16	-	-	Cytoskeletal associated
Rab5b	14	-	-	GTPase
Rac1	14	-	-	GTPase
Ubiquitin-conjugating enzyme E2N	12	-	-	UQ/Proteasome system
Solute carrier family 29	11	3	-	Transporter
Rab18	10	-	-	GTPase
Tropomyosin 3	10	-	-	Cytoskeletal associated
Rab8b	10	-	-	GTPase

analysis. The uninfected, iRBC and post-rupture vesicle membranes were first delipidated by incubating with sodium acetate/ethanol for 1 h at room temperature, which enhanced the recovery of peptides in the subsequent LC/MS analysis (23). The polypeptides were then separated by SDS-PAGE and stained with colloidal Coomassie. Initially we observed that the uninfected RBC and the iRBC membrane proteome migration pattern by Coomassie to be comparable, apart from a major reduction in spectrin band intensity in the iRBC membrane sample. However, the migration pattern for the postrupture vesicle membrane proteome was markedly different (Fig. 3A).

Thirty-four individual gel slices were excised throughout the SDS-PAGE lanes in order to identify proteins and assess their relative size for each of the three proteomes (as graphically depicted in Fig. 3A). Each excised gel band was digested with trypsin, peptides were analyzed by LC/MS/MS, and peptides were matched to proteins using SEQUEST. A total of 33,386 entries from the NCBI database were searched for protein identification. Proteins that had at least three peptides from a minimum of two independent MS analyses were considered as confidence “hits.” Most data sets had a false discovery rate of <2. Although the Coomassie stained gels only revealed a few major proteins, we identified ~250 proteins from each sample (Fig. 5B, see supplemental Table S1A, B, C for complete lists), which is commensurate with prior proteomic studies of human RBCs (23); thus most proteins were present at a level below the level of detection by Coomassie. Furthermore, proteins identified were well distributed throughout the SDS-PAGE gel (Fig. 3B). Spectral counting analysis was used to compare the ratios of total protein abundance, which revealed that only ~15% of the protein hits changed more than threefold (first two bars in histogram), whereas the relative abundance of the remaining ~85% of proteins was within threefold (0.3–1 and 1–3) among all three proteome samples. This data indicates that although the Coomassie stained gels showed

different patterns—primarily because of huge losses of a few major RBC membrane proteins such as spectrins—the abundance of the majority of iRBC membrane proteins remained unchanged during parasite egress (Fig. 3C).

Adducin is Lost from the Host Cytoskeleton 10–15 h before Parasite Egress—In comparing the proteomes of uninfected RBCs and iRBCs, we observed that a subset of host proteins identified with high confidence in the uninfected membrane samples were absent or highly reduced (>>threefold change) in both the iRBC and postrupture vesicle membranes (Table I), suggesting that major cytoskeletal modifications may be occurring far earlier in the erythrocytic life cycle. We observed that erythrocyte adducins, tropomyosin and Rac1 disappear from the membrane fraction around 35 hpi, which was striking as these proteins have been shown to be important for the integrity of the cytoskeleton (26). Direct loss of adducin via mutations or through the loss of Rac1/2 has been shown to disrupt spectrin and actin junctions, (26) leading to spherocytosis and increased hemolysis in *in vivo* mouse models (27, 28). Western blot analysis of iRBC membrane fractions confirmed that α -adducin is present through the first two-thirds of the intraerythrocytic life cycle but is lost from the host cytoskeleton at ~35 hpi (Fig. 4A). This data was corroborated using immunofluorescence, which showed that adducin is localized to the plasma membrane of uninfected and early stage iRBCs (up to 30 hpi), but disappeared around 35 hpi (Fig. 4B). Uninfected RBCs also showed an abundance of cytoplasmic adducin staining, which is diminished in infected cells possibly because of parasite digestion of host cytoplasm. We also show that adducin loss from the cytoskeleton is not dependent on calpain, as calpastatin loading into hypotonically lysed and resealed RBCs did not prevent adducin loss from the membrane fractions of iRBCs by Western blot analysis (Fig. 4C). The loss of α -adducin, as well as tropomyosin and Rac1 after schizogony suggests that cytoskeletal

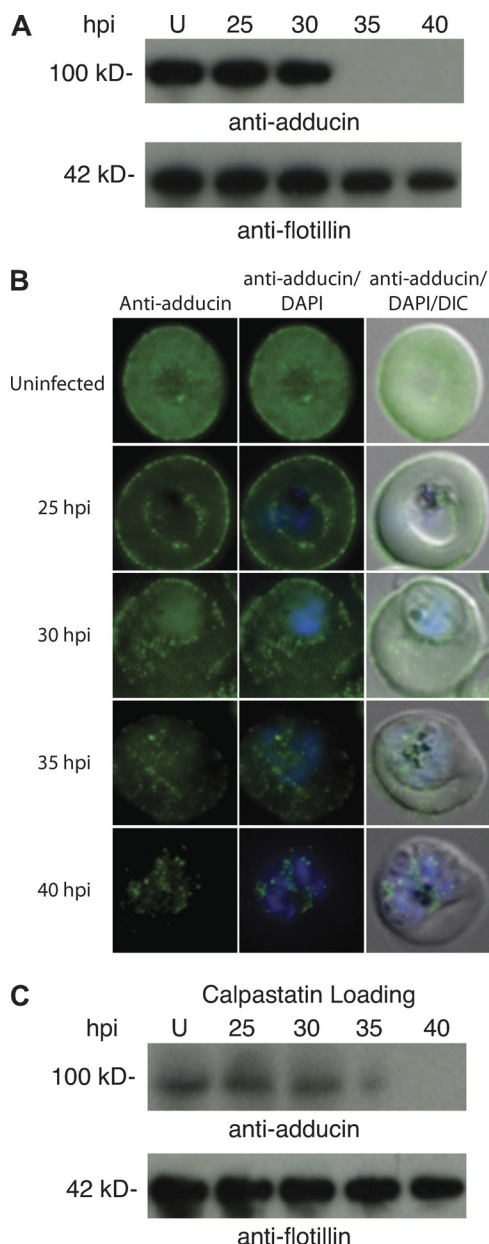


FIG. 4. Loss of adducin from the erythrocyte cytoskeleton prior to parasite escape is calpain-independent. *A*, Western blot analysis confirmed the loss of adducin from the membrane fraction of iRBCs by 35 h postinvasion. Stomatin levels are shown as a loading control. *B*, Immunofluorescence confirms the presence of adducin in uninfected, ring, and trophozoite infected erythrocytes, and its absence in schizont-infected erythrocytes. *C*, Western blot analysis of calpastatin-loaded iRBCs confirms that the loss of adducin from the iRBC cytoskeleton around 35 hpi is calpain-independent.

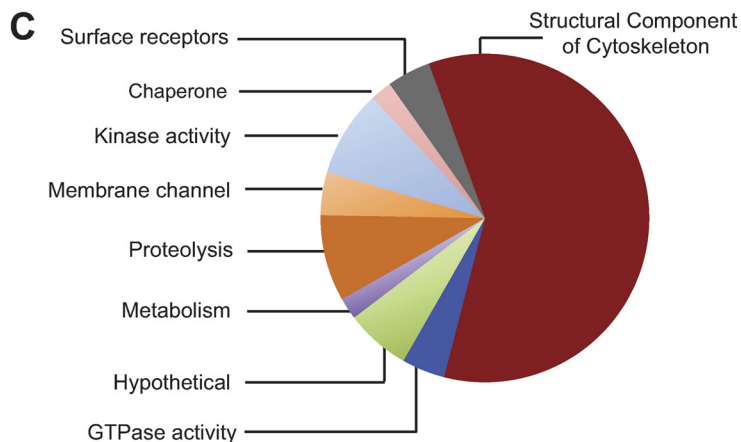
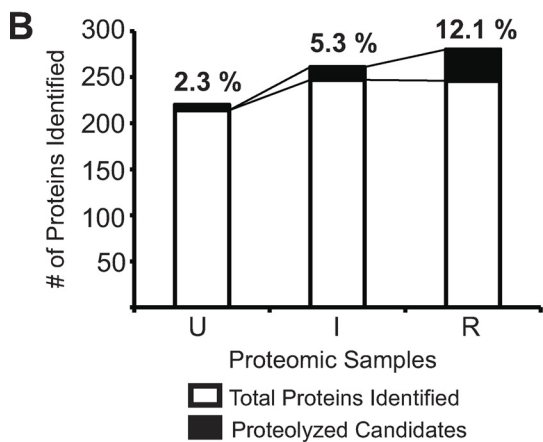
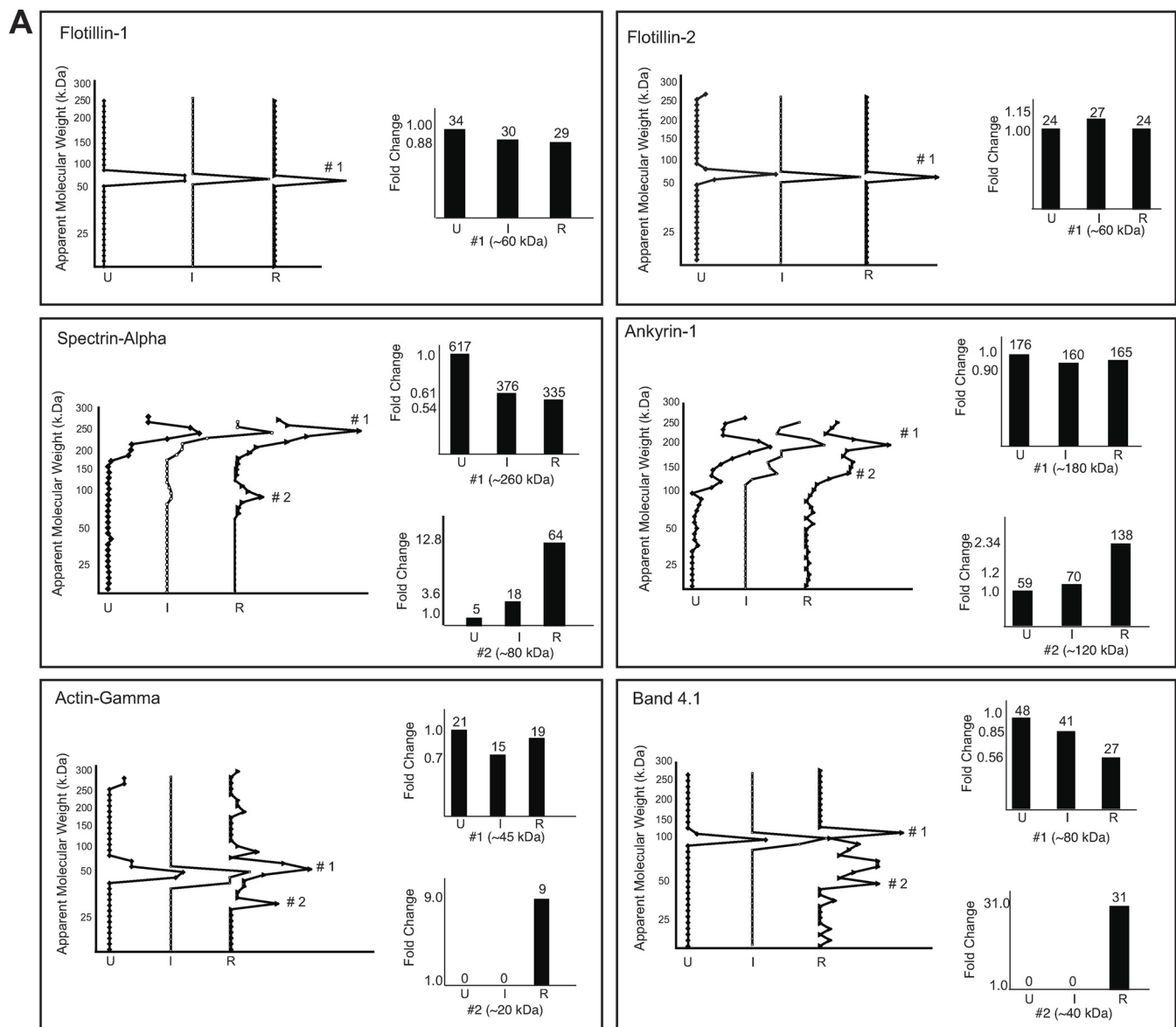
dismantling in preparation for egress begins much earlier than previously thought.

Analysis of Proteome Changes Reveals Global Proteolysis of the Host Cytoskeleton During Parasite Egress—Considering the previously posed role of proteases in parasite egress, we next focused our analysis of the proteomic data on pro-

teins that appeared to be proteolyzed during egress. To do this, we searched for proteins that appeared at significantly smaller sizes than expected in the postrupture vesicle membrane proteome compared with the iRBC and uninfected RBC proteomes, as they likely represented proteins proteolytically processed during parasite egress. We used several overlapping methods to determine proteins that appeared smaller in size. Spectral counts for each protein were plotted against their position in the actual gel lane to create “chromatograms” representing their migration pattern in the SDS-PAGE gel (Fig. 5A) for each proteome, which provided a simple yet efficient tool to compare progressive changes in protein distribution patterns between the three proteomes. Although cytoskeletal proteins such as α -spectrin, ankyrin, actin, and band 4.1 were identified at their expected molecular weight in the iRBC sample, these proteins were also detected at lower molecular weight areas of the chromatogram in the postrupture vesicle membrane samples, suggesting that they had been proteolyzed. It is worth noting that ankyrin had been previously shown to be proteolyzed by crude parasite lysates (29). However, the majority of proteins, such as flotillin-1 and -2, showed no apparent cleavage, as shown by the lack of any low-molecular weight fragments (Fig. 5A, top panel). This revealed that although several proteins from the postrupture vesicle membrane proteome appeared smaller than their predicted size (Fig. 5A, lower panel), the majority of proteins did not undergo any proteolytic cleavage during rupture and appeared at their expected molecular weight in all three proteome samples.

Using this method, we estimated the number of proteolyzed proteins in all three proteomes. We observed a doubling in the number of proteolyzed proteins (2% to 5%) from uninfected to iRBC membrane proteome, however, the magnitude of proteolysis was significantly increased in the post-rupture vesicle proteome (12%) (Fig. 5B). Proteins that had undergone proteolysis were then classified into functional categories: the majority of these proteins (~60%) were associated or members of the cytoskeleton (Fig. 5C, see supplemental Table S2 for a complete list). To date, most of these cytoskeletal proteins have not been reported to be proteolyzed in uninfected RBCs or during *P. falciparum* infection.

To confirm our predictions, we conducted Western blot analysis of potential proteolyzed hits over a timecourse throughout the parasite life cycle (10-hour increments from 10–40 hpi), in comparison to uninfected RBCs (U) and postrupture vesicles (R). Processing of several proteins at the time of rupture that were found to be proteolyzed from the MS data were confirmed, including the key cytoskeletal proteins α/β -spectrins and ankyrin-1 (Fig. 6A), as fragments appeared in the post-rupture lane that were similar in size to those found in the MS analysis (see Fig. 5A). Also, it appeared that integral membrane proteins such as Band 3 were more resistant to proteolysis (data not shown), which may be because of their transmembrane localization rather than peripheral attachment



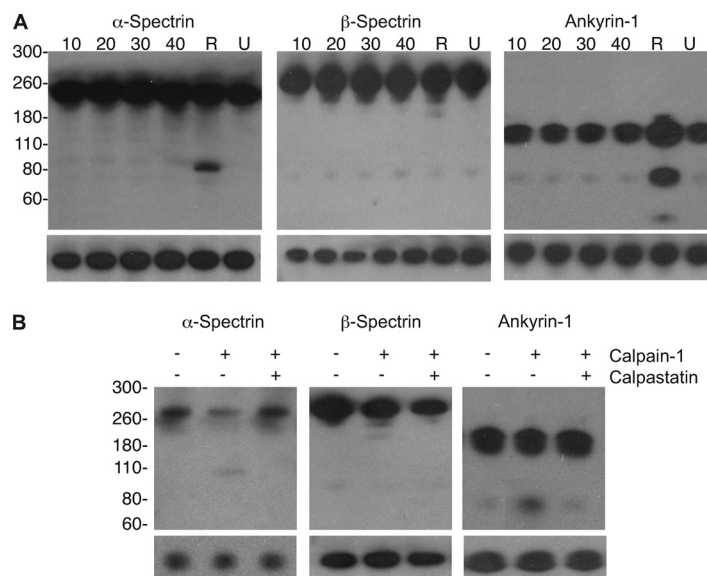


FIG. 6. Validation of calpain-dependent cytoskeletal processing during parasite rupture. *A*, Western blot analysis from uninfected RBC (U), iRBC throughout the life cycle (10–40 hpi), and postrupture vesicle (R) membranes was used to validate the proteolytic processing of candidate proteins. Analysis of α -spectrin, β -spectrin, and ankyrin-1 showed major degradation of target proteins only in the postrupture vesicle proteome sample whereas many proteins, such as flotillin (shown as loading controls underneath each blot) showed no proteolytic processing. *B*, RBC membranes treated for 30 min with activated human calpain-1 were able to recapitulate the processing observed in postrupture vesicles. Western blot analysis of calpain-mediated processing is shown for α -spectrin, β -spectrin, and ankyrin-1.

to the cytoskeleton, making them less accessible to proteases. Several lipid raft-associated proteins including the flotillins were protected from proteolysis, and served as loading controls for the rest of the Western blots shown in Fig. 6A.

We also identified the presence of several proteases in the iRBC proteome (Table II). Notable among these was host calpain-1 that was present only in the late-stage iRBC membranes and postrupture vesicle membranes. Calpain-1 activation and its corresponding translocation to the membrane are important for malaria parasite egress, as we described recently (15). We investigated whether calpain activity could account for the degradation of much of the observed cytoskeletal proteolysis during parasite egress, via incubation with RBC membrane fractions in the presence of Ca^{2+} for 30 min. We provide *in vitro* data validating that, indeed, activated calpain-1 can cleave a whole spectrum of cytoskeletal proteins, generating fragments of similar size to those found in our MS and Western blot analyses of postrupture vesicles (Fig. 6B). In addition to calpain-1, parasite-derived SERA proteins, which have been postulated to have a role in egress,

were abundantly found in our iRBC and postrupture vesicle membrane samples (14).

DISCUSSION

P. falciparum egress is thought to take place in seconds at the end of the 48-hour erythrocytic cycle through the complete destruction of the host RBC. This process is thought to be mediated by parasite proteins such as proteases (10–13), a perforin-like protein (18), and osmotic forces from the growing parasites (8, 30). From our prior work demonstrating that parasites require human calpain (15), we hypothesized that host calpain is used to destabilize the RBC membrane. In this work, we endeavored to provide a more global understanding of changes that occur to the host RBC membrane proteome during parasite egress.

The appearance of large holes in the spectrin network from AFM images of infected RBCs and also of postrupture vesicles showing broken fragments of cytoskeletal structures suggested at least two steps affecting the host cytoskeleton during parasite egress. Our proteomic data revealed that sev-

FIG. 5. Proteomic profiling shows extensive cytoskeletal protein proteolysis during parasite egress. *A*, To determine proteins that were proteolytically processed, the spectral count for each protein was plotted against the corresponding gel slice number (and hence the apparent molecular weight) judged from its migration in the SDS-PAGE gel. Several proteins appeared smaller than their expected molecular weight as indicated by a second peak in the chromatogram corresponding to a lower molecular weight as seen in α -spectrin, band 4.1 and actin. Abundance of the smaller species was universally increased in the postrupture vesicle proteome sample. Otherwise, the majority of the proteins showed no major difference in abundance and molecular weight as exemplified by flotillin-1. *B*, Proteolysis of host membrane proteins significantly increases at egress. Number of processed proteins identified from the uninfected (U), iRBC (I), and postrupture vesicle (R) membrane proteomes is expressed as a percentage of total proteins identified. *C*, Proteins that were processed in the post-rupture vesicle RBC membrane were classified according to their functions as obtained from the human proteins reference database (www.hprd.org), and corresponding Gene Ontology (GO) annotation.

TABLE II

Proteases identified from iRBC and postrupture vesicle membrane samples. A list of proteases identified with four or more unique peptides from (A) infected and (B) postrupture vesicle membrane proteomes are listed

2A. Proteases identified in the proteomic analyses from iRBC membranes (I)

Protease	Accession	Family	Organism	Peptides
Serine Repeat Antigen-5*	PFB0340c	Cysteine (C1)	<i>P. falciparum</i>	182
Calpain-1, Large subunit	gi 12408656	Cysteine (C2)	<i>H. sapiens</i>	22
Serine Repeat Antigen-6*	PFB0335c	Cysteine (C1)	<i>P. falciparum</i>	12

2B. Proteases identified from postrupture RBC membranes (R)

Protease	Accession	Family	Organism	Peptides
Calpain-1, Large subunit	gi 12408656	Cysteine (C2)	<i>H. sapiens</i>	12
Serine Repeat Antigen-6 ^a	PFB0335c	Cysteine (C1)	<i>P. falciparum</i>	5
Serine Repeat Antigen-5 ^a	PFB0340c	Cysteine (C1)	<i>P. falciparum</i>	4

^a Proteolytic activity has not been demonstrated for these proteins.

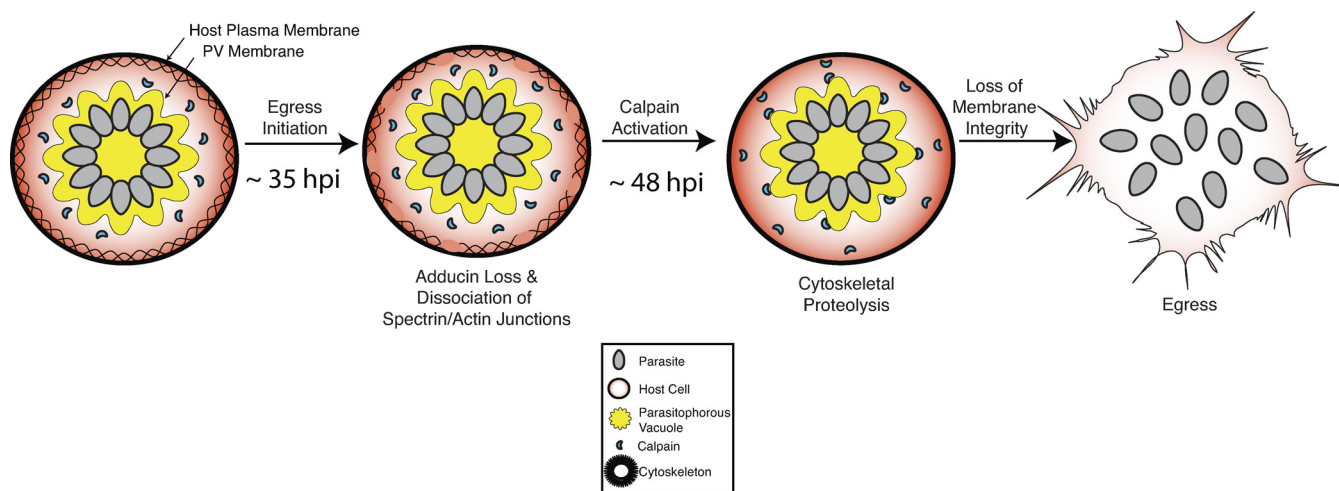


FIG. 7. **New model for parasite driven modifications to the host cytoskeleton during parasite egress.** We propose that parasite egress begins as early as 35 hpi with the loss of spectrin and actin adaptors, and lead to the formation of large holes in the host RBC cytoskeleton, followed by large-scale calpain-mediated proteolysis of the remaining cytoskeleton at 48 hpi to eventually release merozoites.

eral host proteins, including most prominently α/β -adducin, disappeared from the plasma membrane fraction at the time that these large holes appeared in the host RBC cytoskeleton. Targeted disruption of adducin genes has been long known to result increased fragility of the RBC membrane that ultimately leads to spherocytosis and increased hemolysis in mice (27, 28, 31). Thus this initial weakening of the cytoskeleton via the loss of the adducins (perhaps the loss of tropomyosin and Rac1 as well) may be required for the later destruction of membrane integrity to permit facile parasite escape. We determined that α -adducin loss from the RBC cytoskeleton is both temporally and mechanistically distinct from the changes enacted on the host cell at the time of egress by host calpain-1. This suggests a new mechanism used by malaria parasites, occurring 15–20 h prior to parasite egress in order to prepare the iRBC for rupture. This process may be mediated by parasite kinases to modify host proteins during egress because phosphorylation of cytoskeletal proteins has been shown to result in progressive changes to the cytoskeletal network (32–34). Though parasite kinases have been shown

to be exported into the host cell (35, 36), a direct link between parasite kinase activity and iRBC cytoskeletal changes during egress has yet to be explored.

In addition to the loss of α -adducin, our proteomics data revealed that a significant proportion of RBC cytoskeletal proteins were proteolyzed upon parasite egress. In fact, in postrupture vesicle membranes, the total amount of spectrins diminished to $\sim 10\%$ of that found in uninfected RBC membranes. In total, more than 60% of the proteins that were found to be proteolyzed were associated with the host cytoskeleton including most prominently the spectrins, ankyrin, and actin, suggesting that global and pathological proteolysis of the host cytoskeleton occurs during the parasite egress process (~ 48 hpi). Several proteases were also found associated with the iRBC and postrupture vesicle membranes, including host calpain-1, an essential enzyme that apicomplexan parasites utilize for egress (15). We show that calpain-1 can proteolyze most cytoskeletal proteins during egress, which likely accounts for the striking breakdown of the host RBC membrane around the parasite. Although calpain-1 is

capable of proteolyzing many of the cytoskeletal proteins, it is possible that other putative parasite proteases such as SERA family proteases can also perform this function; importantly, SERA5/6 were found to be in abundance on iRBC membranes and postrupture vesicles. Although there is little data concerning the proteolytic activity of SERA proteins or for their direct role during parasite egress from the RBC, it is also possible that they contribute to the egress process through destabilization of the host membrane via a nonproteolytic role.

Together, these data suggest that parasite egress does not occur as a single explosive event just at the end of the 48-hour life cycle. More accurately, the distinct events of cytoskeletal dismantling, which we now demonstrate, suggest a systematic preparation for egress that takes place over at least 15–20 h in which the parasite gradually disrupts the cytoskeleton to ultimately allow for facile escape (Fig. 7). Based on this work, further investigation of parasite proteins (*i.e.* SERAs or parasite kinases) secreted into the host PV or RBC space should be analyzed for potential functions during egress.

Acknowledgments—M. G. M. performed *P. falciparum* experiments, adducin experiments, bioinformatics analysis, and assisted with writing of manuscript. R. C. performed *P. falciparum* experiments and proteomics experiments, and assisted with writing of manuscript. A. P. performed bioinformatics analysis. A. W. performed the LC/MS/MS analysis. H. S. performed AFM imaging. C. D. performed microscopy experiments and maintained parasite cultures. C. T. L. analyzed and verified the AFM data. D. C. G. designed the study, analyzed, assisted in all data interpretation, and wrote the manuscript. We thank I. Blair for allowing access to mass spectrometry instrumentation and D. W. Speicher and P. R. Preiser for helpful discussions. Gino. V. Limmon's help in data presentation is acknowledged. We also thank the Global Enterprise for Micro-Mechanics and Molecular Medicine (GEM⁴) Lab at the National University of Singapore for the use of the Atomic Force Microscope.

* This work was supported by the Penn Genome Frontiers Institute, Penn Institute for Translational Medicine and Therapeutics and the Ritter Foundation (DCG) and NIH5T32AI007532 (MGM).

☐ This article contains [supplemental Tables S1 and S2](#).

** To whom correspondence should be addressed: Department of Pharmacology, University of Pennsylvania, 433 S. University Ave, 304G Lynch Lab, Philadelphia, PA, 19104. Tel.: 215-746-2992; Fax: 215-746-6697; E-mail: dorong@upenn.edu.

¶ Current address: Interdisciplinary Research Group (Infectious Diseases), Singapore-MIT Alliance for Research and Technology (SMART), Centre for Life Sciences, S16-05-06, 28 Medical Drive, Singapore 117456.

|| authors share co-first authorship.

Author Information. The authors declare no competing financial interests. Correspondence and requests for materials should be addressed to D.C. Greenbaum. (e-mail: dorong@upenn.edu).

REFERENCES

- Hay, S. I., Guerra, C. A., Gething, P. W., Patil, A. P., Tatem, A. J., Noor, A. M., Kabaria, C. W., Manh, B. H., Elyazar, I. R., Brooker, S., Smith, D. L., Moyeed, R. A., and Snow, R. W. (2009). A world malaria map: *Plasmodium falciparum* endemicity in 2007. *PLoS Med.* **6**, e1000048
- Maier, A. G., Rug, M., O'Neill, M. T., Brown, M., Chakravorty, S., Szestak, T., Chesson, J., Wu, Y., Hughes, K., Coppel, R. L., Newbold, C., Beeson, J. G., Craig, A., Crabb, B. S., and Cowman, A. F. (2008) Exported proteins required for virulence and rigidity of *Plasmodium falciparum*-infected human erythrocytes. *Cell* **134**, 48–61
- Sherman, I. W., Crandall, I., and Smith, H. (1992) Membrane proteins involved in the adherence of *Plasmodium falciparum*-infected erythrocytes to the endothelium. *Biol. Cell* **74**, 161–178
- Smith, H., Crandall, I., Prudhomme, J., and Sherman, I. W. (1992) Optimization and inhibition of the adherent ability of *Plasmodium falciparum*-infected erythrocytes. *Mem. Inst. Oswaldo Cruz.* **87 Suppl 3**, 303–312
- Crabb, B. S., Cooke, B. M., Reeder, J. C., Waller, R. F., Caruana, S. R., Davern, K. M., Wickham, M. E., Brown, G. V., Coppel, R. L., and Cowman, A. F. (1997) Targeted gene disruption shows that knobs enable malaria-infected red cells to cytoadhere under physiological shear stress. *Cell* **89**, 287–296
- Marti, M., Baum, J., Rug, M., Tilley, L., and Cowman, A. F. (2005) Signal-mediated export of proteins from the malaria parasite to the host erythrocyte. *J. Cell Biol.* **171**, 587–592
- Hiller, N. L., Bhattacharjee, S., van Ooij, C., Liolios, K., Harrison, T., Lopez-Estraño, C., and Haldar, K. (2004) A host-targeting signal in virulence proteins reveals a secretome in malarial infection. *Science* **306**, 1934–1937
- Glushakova, S., Yin, D., Li, T., and Zimmerberg, J. (2005) Membrane transformation during malaria parasite release from human red blood cells. *Curr. Biol.* **15**, 1645–1650
- Hadley, T., Aikawa, M., and Miller, L. H. (1983) *Plasmodium knowlesi*: studies on invasion of rhesus erythrocytes by merozoites in the presence of protease inhibitors. *Exp. Parasitol.* **55**, 306–311
- Salmon, B. L., Oksman, A., and Goldberg, D. E. (2001) Malaria parasite exit from the host erythrocyte: a two-step process requiring extraerythrocytic proteolysis. *Proc. Natl. Acad. Sci. U.S.A.* **98**, 271–276
- Wickham, M. E., Culvenor, J. G., and Cowman, A. F. (2003) Selective inhibition of a two-step egress of malaria parasites from the host erythrocyte. *J. Biol. Chem.* **278**, 37658–37663
- Glushakova, S., Mazar, J., Hohmann-Marriott, M. F., Hama, E., and Zimmerberg, J. (2009) Irreversible effect of cysteine protease inhibitors on the release of malaria parasites from infected erythrocytes. *Cell Microbiol.* **11**, 95–105
- Arastu-Kapur, S., Ponder, E. L., Fonović, U. P., Yeoh, S., Yuan, F., Fonović, M., Grainger, M., Phillips, C. I., Powers, J. C., and Bogoy, M. (2008) Identification of proteases that regulate erythrocyte rupture by the malaria parasite *Plasmodium falciparum*. *Nat. Chem. Biol.* **4**, 203–213
- Yeoh, S., O'Donnell, R. A., Koussis, K., Dluzewski, A. R., Ansell, K. H., Osborne, S. A., Hackett, F., Withers-Martinez, C., Mitchell, G. H., Bannister, L. H., Bryans, J. S., Kettleborough, C. A., and Blackman, M. J. (2007) Subcellular discharge of a serine protease mediates release of invasive malaria parasites from host erythrocytes. *Cell* **131**, 1072–1083
- Chandramohanadas, R., Davis, P. H., Beiting, D. P., Harbut, M. B., Darling, C., Velmourougane, G., Lee, M. Y., Greer, P. A., Roos, D. S., and Greenbaum, D. C. (2009) Apicomplexan parasites co-opt host calpains to facilitate their escape from infected cells. *Science* **324**, 794–797
- Glushakova, S., Humphrey, G., Leikina, E., Balaban, A., Miller, J., and Zimmerberg, J. (2010) New stages in the program of malaria parasite egress imaged in normal and sickle erythrocytes. *Curr. Biol.* Jun 22; **20**(12):1117–1121
- Nagamune, K., Hicks, L. M., Fux, B., Brossier, F., Chini, E. N., and Sibley, L. D. (2008) Abscisic acid controls calcium-dependent egress and development in *Toxoplasma gondii*. *Nature* **451**, 207–210
- Kafsack, B. F., Pena, J. D., Coppens, I., Ravindran, S., Boothroyd, J. C., and Carruthers, V. B. (2009) Rapid membrane disruption by a perforin-like protein facilitates parasite exit from host cells. *Science* **323**, 530–533
- Dvorin, J. D., Martyn, D. C., Patel, S. D., Grimley, J. S., Collins, C. R., Hopp, C. S., Bright, A. T., Westenberger, S., Winzeler, E., Blackman, M. J., Baker, D. A., Wandless, T. J., and Duraisingh, M. T. (2010) A plant-like kinase in *Plasmodium falciparum* regulates parasite egress from erythrocytes. *Science* **328**, 910–912
- Bowyer, P. W., Simon, G. M., Cravatt, B. F., and Bogoy, M. (2010) Global profiling of proteolysis during rupture of *P. falciparum* from the host erythrocyte. *Mol. Cell. Proteomics* **5**, M110.001636
- Trager, W., and Jensen, J. B. (1976) Human malaria parasites in continuous culture. *Science* **193**, 673–675
- Liu, F., Burgess, J., Mizukami, H., and Ostafin, A. (2003) Sample preparation and imaging of erythrocyte cytoskeleton with the atomic force mi-

- croscopy. *Cell Biochem. Biophys.* **38**, 251–270
23. Pasini, E. M., Kirkegaard, M., Mortensen, P., Lutz, H. U., Thomas, A. W., and Mann, M. (2006) In-depth analysis of the membrane and cytosolic proteome of red blood cells. *Blood* **108**, 791–801
24. Greenbaum, D. C., Baruch, A., Grainger, M., Bozdech, Z., Medzihradsky, K. F., Engel, J., DeRisi, J., Holder, A. A., and Bogoy, M. (2002) A role for the protease falcipain 1 in host cell invasion by the human malaria parasite. *Science* **298**, 2002–2006
25. Shevchenko, A., Tomas, H., Havlis, J., Olsen, J. V., and Mann, M. (2006) In-gel digestion for mass spectrometric characterization of proteins and proteomes. *Nat. Protoc.* **1**, 2856–2860
26. Kalfa, T. A., Pushkaran, S., Mohandas, N., Hartwig, J. H., Fowler, V. M., Johnson, J. F., Joiner, C. H., Williams, D. A., and Zheng, Y. (2006) Rac GTPases regulate the morphology and deformability of the erythrocyte cytoskeleton. *Blood* **108**, 3637–3645
27. Robledo, R. F., Ciciotte, S. L., Gwynn, B., Sahr, K. E., Gilligan, D. M., Mohandas, N., and Peters, L. L. (2008) Targeted deletion of alpha-adducin results in absent beta- and gamma-adducin, compensated hemolytic anemia, and lethal hydrocephalus in mice. *Blood* **112**, 4298–4307
28. Gilligan, D. M., Lozovatsky, L., Gwynn, B., Brugnara, C., Mohandas, N., and Peters, L. L. (1999) Targeted disruption of the beta adducin gene (Add2) causes red blood cell spherocytosis in mice. *Proc. Natl. Acad. Sci. U.S.A.* **96**, 10717–10722
29. Raphael, P., Takakuwa, Y., Manno, S., Liu, S. C., Chishti, A. H., and Hanspal, M. (2000) A cysteine protease activity from *Plasmodium falciparum* cleaves human erythrocyte ankyrin. *Mol Biochem. Parasitol.* **110**, 259–272
30. Lew, V. L., Macdonald, L., Ginsburg, H., Krugliak, M., and Tiffert, T. (2004) Excess haemoglobin digestion by malaria parasites: a strategy to prevent premature host cell lysis. *Blood Cells Mol. Dis.* **32**, 353–359
31. Chen, H., Khan, A. A., Liu, F., Gilligan, D. M., Peters, L. L., Messick, J., Haschek-Hock, W. M., Li, X. R., Ostafin, A. E., and Chishti, A. H. (2007) Combined deletion of mouse dematin-head piece and beta-adducin exerts a novel effect on the spectrin-actin junctions leading to erythrocyte fragility and hemolytic anemia. *J. Biol. Chem.* **282**, 4124–4135
32. Lu, P. W., Soong, C. J., and Tao, M. (1985) Phosphorylation of ankyrin decreases its affinity for spectrin tetramer. *J. Biol. Chem.* **260**, 14958–14964
33. Soong, C. J., Lu, P. W., and Tao, M. (1987) Analysis of band 3 cytoplasmic domain phosphorylation and association with ankyrin. *Arch Biochem. Biophys.* **254**, 509–517
34. Manno, S., Takakuwa, Y., Nagao, K., and Mohandas, N. (1995) Modulation of erythrocyte membrane mechanical function by beta-spectrin phosphorylation and dephosphorylation. *J. Biol. Chem.* **270**, 5659–5665
35. Vaid, A., Ranjan, R., Smythe, W. A., Hoppe, H. C., and Sharma, P. (2010) PfPI3K, a phosphatidylinositol-3 kinase from *Plasmodium falciparum*, is exported to the host erythrocyte and is involved in hemoglobin trafficking. *Blood* **115**, 2500–2507
36. Nunes, M. C., Goldring, J. P., Doerig, C., and Scherf, A. (2007) A novel protein kinase family in *Plasmodium falciparum* is differentially transcribed and secreted to various cellular compartments of the host cell. *Mol. Microbiol.* **63**, 391–403